

This discussion paper is/has been under review for the journal Atmospheric Chemistry and Physics (ACP). Please refer to the corresponding final paper in ACP if available.

Estimating the atmospheric boundary layer height over sloped, forested terrain from surface spectral analysis during BEARPEX

W. Choi¹, I. C. Faloona¹, M. McKay^{2,*}, A. H. Goldstein², and B. Baker³

¹University of California, Davis, Dept. of Land, Air, and Water Resources, Davis, California, USA

²University of California, Berkeley, Dept. of Environmental Science, Policy and Management, Berkeley, California, USA

³California State University, Sacramento, Dept. of Chemistry, California, USA

* now at: California Air Resources Board, Sacramento, California, USA

Received: 9 August 2010 – Accepted: 5 October 2010 – Published: 2 November 2010

Correspondence to: W. Choi (wschoi@ucdavis.edu)

Published by Copernicus Publications on behalf of the European Geosciences Union.

Estimating the atmospheric boundary layer height over sloped

W. Choi et al.

Title Page

Abstract

Introduction

Conclusions

References

Tables

Figures

⏪

⏩

◀

▶

Back

Close

Full Screen / Esc

Printer-friendly Version

Interactive Discussion

Abstract

In this study the atmospheric boundary layer (ABL) height (z_i) over complex, forested terrain is estimated based on the power spectra and the integral length scale of horizontal winds obtained from a three-axis sonic anemometer during the BEARPEX (Biosphere Effects on Aerosol and Photochemistry) Experiment. The z_i values estimated with this technique showed very good agreement with observations obtained from balloon tether sonde (2007) and rawinsonde (2009) measurements under unstable conditions ($z/L < 0$) at the coniferous forest in the California Sierra Nevada. The behavior of the nocturnal boundary layer height (h) and power spectra of lateral winds and temperature under stable conditions ($z/L > 0$) is also presented. The nocturnal boundary layer height is found to be fairly well predicted by a recent interpolation formula proposed by Zilitinkevich et al. (2007), although it was observed to only vary from 60–80 m during the experiment. Finally, significant directional wind shear was observed during both day and night with winds backing from the prevailing west-southwesterlies in the ABL (anabatic cross-valley circulation) to consistent southerlies in a layer ~ 1 km thick just above the ABL before veering to the prevailing westerlies further aloft. We show that this is consistent with the forcing of a thermal wind driven by the regional temperature gradient directed due east in the lower troposphere.

1 Introduction

The depth of the lower atmospheric mixing layer, or boundary layer height (z_i), is one of the most important meteorological parameters, not only affecting the distribution of reactive atmospheric chemicals but also playing a key role in air quality assessment at the local or regional scale (Seibert et al., 2000). The distributions of reactive atmospheric species, such as some volatile organic compounds (VOCs), are strongly influenced by atmospheric boundary layer (ABL) turbulence and its vertical extent, z_i , because these compounds are in general emitted from the surface, or produced secondarily

ACPD

10, 25759–25801, 2010

Estimating the atmospheric boundary layer height over sloped

W. Choi et al.

Title Page

Abstract

Introduction

Conclusions

References

Tables

Figures

⏪

⏩

◀

▶

Back

Close

Full Screen / Esc

Printer-friendly Version

Interactive Discussion



Estimating the atmospheric boundary layer height over sloped

W. Choi et al.

Title Page

Abstract

Introduction

Conclusions

References

Tables

Figures



Back

Close

Full Screen / Esc

Printer-friendly Version

Interactive Discussion



within the ABL, possessing lifetimes similar to or shorter than the time scales associated with the largest eddies confined by z_i . In addition, it is essential to determine the stable nocturnal boundary layer (NBL) height (h), because the impact of dry deposition on chemical species budgets at night is determined by h , and dry deposition can be a major loss mechanism for many reaction products that are mainly decomposed by photolysis and/or the reaction with OH in the daytime (e.g., H_2CO , O_3 , peroxy acyl nitrates, VOCs). Moreover, the transport and dispersion of atmospheric trace gases and particles strongly depend on the state of the atmospheric boundary layer such as stability and z_i (Kossmann et al., 1998). Therefore, it is also very important to determine z_i in regional transport/dispersion models for air pollution assessments as well as for quantifying the budget of atmospheric trace gases.

Several conventions for the determination of z_i have been developed, typically based on the characteristics of the profiles of the mean wind speed (\bar{U}), mean potential temperature ($\bar{\theta}$), standard deviation of the vertical wind-speed (σ_w), and bulk Richardson number (Ri_b) obtained by sonde and aircraft measurements (Hanna, 1969; Liu and Ohtaki, 1997; Seibert et al., 2000; Stull, 1988; Zeng et al., 2004). Other methods are based on the detection of discontinuities in backscattered energy by acoustic, microwave, and optical techniques that can be associated with entrainment around the inversion base (Angevine et al., 1994; Kaimal et al., 1982). Nonetheless, it is not simple to measure z_i at any given site and time due to limited resources. Thus, it is common in many atmospheric chemistry and transport studies to resort to assumptions about z_i based on previous model results or measurements made at other locations with similar surface conditions (Dillon et al., 2002; Day et al., 2008).

Since the early 1970s, it has been recognized that surface layer, or Monin-Obukhov similarity does not accurately describe the behavior of horizontal wind fluctuations observed near the surface; rather, their statistical properties appear to contain information about the largest, ABL-filling eddies of the flow (Wyngaard, 1988). Subsequently the use of fast anemometers in determining z_i based on empirical relationships with the statistics of horizontal winds has developed gradually from both aircraft and tower

investigations (Liu and Ohtaki, 1997; Oncley et al., 2004; Kaimal et al., 1982, 1978; Hojstrup, 1982). Although most studies of z_i by spectral analysis of the vertical and horizontal winds have been conducted by aircraft measurements, or limited to open and flat uniform terrain, this technique can be useful in exploring ABL characteristics more widely because of the increased prevalence in recent years of the eddy covariance technique in making air-surface exchange measurements. Here we present the empirical relationships of spectral peak frequency and integral length scale of horizontal winds to z_i above the canopy of a ponderosa pine forest in the California Sierra Nevada found during the two BEARPEX campaigns of 2007 and 2009 under convective conditions. Spectral analyses and discussions for the stable nocturnal boundary layers (from 2009) are also presented, and shown to exhibit fair correspondence with the parameterization recently suggested by Zilitinkevich et al. (2007) that depends on the Coriolis parameter, friction velocity, Obukhov length, and the buoyancy frequency directly above the NBL.

2 Theory and methods

While the vertical winds feel the presence of the surface and thus scale with the height above the ground, ABL-filling eddies dominate the horizontal wind gusts (Wyngaard, 2010). Although the mean horizontal wind speed is strongly influenced by the surface, its variability scales with the largest ABL-filling eddy sizes that are confined to z_i (Panofsky et al., 1977). The daytime boundary layer develops as the surface warms due to solar heating, producing a buoyancy flux, and hence the spectral density in the turbulent kinetic energy (TKE) production region correspondingly develops. The largest ABL-filling eddy sizes further increase as the boundary layer grows, because the greater mixed depths generally provide more space for the largest eddies to develop above the heated surface. Assuming Taylor's frozen wave hypothesis (Taylor, 1938), the eddy sizes, which are represented by wavelength (λ), can be converted to a frequency scale with the mean wind speed as $f(s^{-1}) = \overline{U}(m \cdot s^{-1})/\lambda(m)$ (Stull, 1988).

Estimating the atmospheric boundary layer height over sloped

W. Choi et al.

Title Page

Abstract

Introduction

Conclusions

References

Tables

Figures



Back

Close

Full Screen / Esc

Printer-friendly Version

Interactive Discussion



Estimating the atmospheric boundary layer height over sloped

W. Choi et al.

Title Page

Abstract

Introduction

Conclusions

References

Tables

Figures



Back

Close

Full Screen / Esc

Printer-friendly Version

Interactive Discussion



Consequently, it is expected that the frequency of maximum spectral density will tend to decrease as the boundary layer develops, and as the static stability grows more unstable (Hojstrup, 1982; Panofsky and Dutton, 1984). Thus the variance of the horizontal wind, which represents the bulk of the turbulent kinetic energy in the surface layer, scales with z_i (Banta, 1985), revealing the frequency and therefore size of the largest ABL-filling eddies.

Occasional balloon tethersonde and radiosonde measurements were conducted during the two BEARPEX (Biosphere Effects on Aerosols and Photochemistry Experiment) campaigns in 2007 (15 August to 10 October) and 2009 (15 June to 31 July), respectively. The experiments took place at the Blodgett Forest Research Station (BFRS) located on the western slope of the Sierra-Nevada Mountains in California (38.9° N, 120.6° W; 1315 m elevation). Blodgett is a managed forest, mainly consisting of conifer trees (30% of ground area) dominated by *Pinus ponderosa* L. with individuals of Douglas fir, white fir, and incense-cedar, a few oak trees (California black oak; 2%), forbs (7%) and shrubs (*Mazaita* and *Ceanothus*; 25%) (Goldstein et al., 2000; Misson et al., 2005). The canopy around the observation tower during the experiment was relatively homogeneous with mean heights of 7.9 m in 2007 and 8.7 m in 2009. The slope of the surrounding terrain is gentle within ~200 m of the tower site with less than 2° in the north, south, and east. To the west, the slope is steeper varying 0–15° (Goldstein et al., 2000). Total one-side projected leaf area index (LAI) of the overstory near the tower was 3.3 and 3.7 m² m⁻² in 2007 and 2009, respectively. More details concerning the plantation and its terrain are described in Goldstein et al. (2000) and Misson et al. (2005). During the months of these field experiments, an extremely consistent thermally driven cross-valley circulation establishes upslope winds (anabatic southwesterlies) during the daytime, followed by downslope flow (katabatic easterlies) overnight (Dillon et al., 2002).

Observed ABL heights were determined from the vertical profiles of virtual potential temperature, specific (q , g kg⁻¹) and relative humidity (RH, %), and wind speed and direction measured with the balloon tethersonde (Atmospheric Technology Division of

Estimating the atmospheric boundary layer height over sloped

W. Choi et al.

Title Page

Abstract

Introduction

Conclusions

References

Tables

Figures

⏪

⏩

◀

▶

Back

Close

Full Screen / Esc

Printer-friendly Version

Interactive Discussion

NCAR) in 2007 and with rawinsondes (GRAW radiosondes, DFM-06) in 2009. Observations were made in unstable environments of the evolving boundary layer and in the fully developed convective boundary layer (CBL) (08:00 ~ 16:00 PST) in 2007 and further under stratified stable nocturnal conditions (20:00 ~ 05:00 PST) in 2009. Virtual potential temperature was calculated from the pressure difference based on a reference pressure of 1000 mb, and water vapor concentrations measured at that height. The maximum measurement altitude was constrained to <1000 m during BEARPEX 2007 due to the physical limitation of the tether which trailed upslope in the daytime due to the prevailing wind. Nonetheless, the relatively shallow ABL heights at the site were observable in most of the vertical profiles. Compared to summer continental regions at similar latitudes with large surface heat fluxes, low CBL heights are expected at Blodgett, and throughout the Central Valley writ large, due to mesoscale orographic effects (Seaman et al., 1995; Burk and Thompson, 1996). Aside from being influenced by strong subsidence in the lee of the Pacific High throughout the summer months, daytime CBL heights along the western slope of the Sierras are further expected to be relatively shallow because of the low level horizontal divergence induced by the cross-valley thermal circulation as well as advection of z_i aloft in the prevailing westerlies (Kossmann et al., 1998). The Obukhov length scale (L), defined as

$$L \equiv - \frac{u_*^3 \overline{\theta_v}}{\kappa g_0 \overline{(w'\theta'_v)}_s} \quad (1)$$

is used as a general indicator of surface layer stability, usually expressed as the non-dimensional stability parameter, z/L ($z/L > 0$ stable; $z/L = 0$ neutral; $z/L < 0$ unstable) (Stull, 1988). Here u_* is surface friction velocity, θ_v is virtual potential temperature, κ is the von Kármán constant ($\kappa = 0.4$), $\overline{(w'\theta'_v)}_s$ is the surface vertical buoyancy flux, and g_0 is gravitational acceleration. u_* and $\overline{(w'\theta'_v)}_s$ were obtained at the measurement height (12.5 m a.g.l).

A three-axis sonic anemometer (ATI Electronics Inc.) was mounted on the top of the observation tower (Goldstein et al., 2000) at 12.5 m, which is 4.6 m and 3.8 m above the

Estimating the atmospheric boundary layer height over sloped

W. Choi et al.

Title Page

Abstract

Introduction

Conclusions

References

Tables

Figures



Back

Close

Full Screen / Esc

Printer-friendly Version

Interactive Discussion



canopy in 2007 and 2009, respectively, and 3 m out from the tower into the (daytime) upwind direction to measure three directional wind (u -, v -, and w -components) and temperature with 10 Hz time resolution. Wind data were sampled for 90 min runs for the CBL and 30 min runs for the stable NBL conditions to conduct the spectral analyses.

5 The winds were corrected by rotating the anemometer axes such that the mean wind, \bar{u} , is aligned with the x-axis (streamwise), and the mean crosswind (lateral) and vertical wind are zero ($\bar{v} = 0$ and $\bar{w} = 0$). The time series of the corrected winds were converted into spectral density using the fast Fourier transform (FFT). The detailed description for the FFT is described elsewhere (Lenschow and Stankov, 1986; Stull, 1988). Before the
10 transformation, a linear trend is removed from the time series of the horizontal winds.

3 Data analysis

3.1 Observed ABL heights above the canopy of Blodgett Forest

Several definitions to determine the ABL height for unstable air have been suggested in previous studies based on the vertical profiles of virtual potential temperature and/or
15 its (buoyancy) flux: (1) as the height of the heat flux minimum, which in general, corresponds to the middle of the capping inversion layer (Sullivan et al., 1998; Wyngaard and Lemone, 1980; Zeng et al., 2004), (2) as the base of the capping inversion layer (Barnes et al., 1980), (3) as the inversion top (Betts and Albrecht, 1987), and (4) as the height at which the virtual potential temperature is the same as the surface tem-
20 perature (Holzworth, 1964; Seibert et al., 2000). As Seibert et al. (2000) point out, however, definition (4) strongly depends on the surface temperature particularly in the absence of a pronounced capping inversion and is not strongly related to the sharp decrease in trace gas concentrations. The sonde data obtained in this study, in fact, often shows a strong superadiabatic lapse rate in the surface, without a strong cap-
25 ping inversion. The definition (3) is also difficult to apply in the absence of a strong

Estimating the atmospheric boundary layer height over sloped

W. Choi et al.

Title Page

Abstract

Introduction

Conclusions

References

Tables

Figures

⏪

⏩

◀

▶

Back

Close

Full Screen / Esc

Printer-friendly Version

Interactive Discussion

capping inversion. Thus, in this study, we determine the daytime ABL height (z_i) as the middle of the inversion layer that lies above the well mixed boundary layer, as is recommended by Stull (1988). In addition, this definition generally corresponds to definition (1) (Wyngaard and Lemone, 1980). In cases where the middle of the inversion layer was difficult to identify, the inversion base (definition 2) was applied as an alternate. Besides virtual potential temperature (θ_v), profiles of specific (q) and relative humidity (RH), wind speed, the vertical gradient of θ_v ($d\theta_v/dz$), and bulk Richardson number (Ri_b) are also taken into account to determine the best ABL height (z_i) from the sonde measurements. The bulk Richardson number was calculated by Eq. (2), where $\overline{\theta_v}$ is the mean virtual potential temperature, and $\Delta\overline{\theta_v}$, $\Delta\overline{U}$, and Δz are the differences of θ_v , \overline{U} , and vertical distance between two adjacent layers (~ 40 m for unstable air and ~ 4 m for the NBL), respectively. Stull (1988) suggested that a value larger than the critical Richardson number, $Ri_c = 0.25$, should be used to determine the presence of turbulence in a given layer. He also recommends that the probability of clear air turbulence is effectively zero when bulk Ri_b is larger than 10.25.

$$Ri_b = \frac{g\Delta\overline{\theta_v}}{\overline{\theta_v}\Delta z} \cdot \left(\frac{\Delta\overline{U}}{\Delta z} \right)^{-2} \quad (2)$$

The vertical profiles of θ_v , q , RH, winds, $d\theta_v/dz$, and bulk Ri_b for the tether sonde flight, launched at 10:23 PST of 21 August 2007, are shown in Fig. (1), for example. In this case, θ_v starts increasing at 600 m without significant changes in q and wind speed. At 780 m, RH and q drastically decrease with the increase in θ_v , implying the existence of free tropospheric air above. However, $d\theta_v/dz$ shows a local peak (~ 2 K/100 m) at 650 m with Ri_b of 11, which represents stable conditions, although very large Ri_b is also observed above 800 m. In addition, nearly constant RH with height is observed between 600 and 800 m altitude, unlike the vertical changes below 600 m. The local minimum in wind speeds also appears at 750 m with comparably less fluctuations above that height. Based on these vertical variations of observed parameters we determine z_i

at 750 m. z_i for the other tetheredsonde flights were determined in an analogous manner and are shown in Table 1 along with the mean wind speed (\bar{U}) in the surface, surface layer stability (z/L), and friction velocity, u_* , for the periods of the tetheredsonde measurements. The surface layer stability was unstable whenever tetheredsonde measurements were conducted even in the early morning with values (z/L) ranging from 0.03 ~ 0.29.

The NBL height has traditionally been more difficult to quantify exactly because the stable layer in many cases smoothly tapers towards the neutral residual layer above without a distinct marker at the interface. Those difficulties have led to many definitions of NBL height (Stull, 1988). In this study, we determine NBL height as the top of the stable layer, above which $\partial\theta/\partial z \cong 0$, also taking into account the vertical profiles of q and wind. For instance, the vertical profiles of θ_v , q , winds, vertical temperature gradient ($d\theta_v/dz$), and bulk Richardson number (Ri_b) obtained at 01:25 PST of 9 July 2009 are shown in Fig. 2. The surface layer is seen below 15 m, in which the vertical gradient of θ_v is extremely steep (up to 4 K/10 m) due to radiative surface cooling, and water vapor and wind speed sharply increase with height, likely due to the presence of the surface and/or trees such as deposition/condensation to and friction on the surface, respectively.

In order to determine the NBL height, the vertical profiles of $d\theta_v/dz$ and Ri_b as well as θ_v , q , and winds are examined. First of all, the wind direction changes from 90° toward 180° above the NBL height (represented by a gray dashed line in Fig. 2), and the wind speed also increases and becomes more variable. Secondly, the vertical gradient of θ_v gets close to zero around 80 m, although $d\theta_v/dz$, strictly speaking, becomes 0 above 120 m. Lastly, Ri_b below 70 m represents very stable conditions suppressing turbulent flows ($Ri_b > 1$) and nearly neutral above that, implying turbulent flows which may exist in the residual layer (Fig. 2d). Considering all the above vertical variations, the NBL height in this case is determined to be ~80 m. The mean wind speed (\bar{U}) at 12.5 m a.g.l., friction velocity (u_*), $d\ln(\bar{\theta}_v)/dz$ within the NBL, and the Obukhov length (L) as well as the NBL depths are shown in Table 4 during the period of radiosonde measurements in 2009.

Estimating the atmospheric boundary layer height over sloped

W. Choi et al.

[Title Page](#)[Abstract](#)[Introduction](#)[Conclusions](#)[References](#)[Tables](#)[Figures](#)[⏪](#)[⏩](#)[◀](#)[▶](#)[Back](#)[Close](#)[Full Screen / Esc](#)[Printer-friendly Version](#)[Interactive Discussion](#)

3.2 Determination of maximum spectral frequency (n_{\max}) and Integral length scale (Λ)

The energy spectrum in the atmospheric boundary layer shows three distinct regions: (1) the energy containing scales comprising the majority of the variance which are associated with the principal mechanisms of turbulence production (lowest frequency region), (2) a dissipation range wherein molecular viscosity converts kinetic energy to internal energy (highest frequency region), and (3) an inertial subrange where energy is not produced nor dissipated but conducted to smaller scales (between the energy containing and dissipation range) (Kaimal and Finnigan, 1994). The maximum energy in general appears in the energy-containing range of the spectrum because it is related to turbulent kinetic energy production mechanisms such as wind shear and buoyancy forcing. Caughey et al. (1979) showed that the logarithmic spectrum of horizontal wind velocity components (normalized by their integral over the frequency band) can be fit by a single curve, and the wavelength at the maximum spectral density (λ_m) is related to the boundary layer height for stable air ($z/L > 0$) over flat terrain. Oncley et al. (2004) used these relationships to estimate the stable boundary layer height above a snow surface in Antarctica. In addition, Liu and Ohtaki (1997) proposed that the normalized spectral maximum frequency (n_{\max}) of lateral winds can be a good estimate of the CBL depth above a station in the Gobi Desert (flat and open sandy terrain).

n_{\max} can be determined by fitting an analytic form suggested by Kaimal and Finnigan (1994) (Eq. 3), where f is frequency (s^{-1}), n is normalized frequency ($n = f \cdot z_d / U$), z_d is the measurement height corrected by the displacement height (12.5 m – d), and n_{\max} is the normalized frequency at the peak of the spectrum. The displacement height, d , is estimated as $3/4$ of the canopy height (5.9 m and 6.5 m in 2007 and 2009, respectively). B_0 is $1/(r - 1)$, and $r = 5/3$ for the power spectrum (Oncley et al., 2004). Although the form of Eq. (3) was derived for stable air, we found that the power spectra of the cross-stream winds obtained in the early morning, when the convective boundary layer is not fully developed, is explained well by Eq. (3) as shown in Fig. 3a. The

Estimating the atmospheric boundary layer height over sloped

W. Choi et al.

Title Page

Abstract

Introduction

Conclusions

References

Tables

Figures

◀

▶

◀

▶

Back

Close

Full Screen / Esc

Printer-friendly Version

Interactive Discussion

stability parameter, $-z/L$, was observed to be 0.038 at that time, nearly neutral, and n_{\max} ($= 0.06$) is shifted to a lower frequency than the neutral limit approached from stable conditions, which was suggested by Panofsky and Dutton (1984) to be $n_{\max}=0.16$. Considering that the measurements were conducted above a pine forest canopy in sloped terrain, rather than a flat and open surface, and that the observation was made under slightly unstable conditions, the shift of n_{\max} is not surprising (Hojstrup, 1982).

$$\frac{nS(n)}{\sigma^2} = \frac{A_0 (n/n_{\max})}{1 + B_0(n/n_{\max})^r} \quad (3)$$

As the surface layer grows more unstable, and z_i increases due to buoyancy fluxes caused by strong surface heating, n_{\max} appears at progressively lower frequencies. In addition, the power spectrum of the horizontal wind components scales with z_i/L and $n_i = (f \cdot z_i)/U$ due to the effects of low frequency convective eddies (Hojstrup, 1982; Liu and Ohtaki, 1997). In such cases the power spectra of the horizontal winds cannot be described completely by a single curve that covers the largest scales of motion through the inertial subrange. Hojstrup (1982) suggested the power spectrum for horizontal wind components can be expressed by the sum of low-frequency (S_L) and high-frequency (S_H) parts for the unstable CBL. S_L depends on z_i , the Obukhov length (L), and normalized frequency $n_i = (f \cdot z_i)/U$, whereas S_H only depends on $n = (f \cdot z)/U$. However the Hojstrup model does not provide a good tool to estimate λ_m because it contains z_i itself in the independent variable. As shown by Hojstrup (1982), the high-wavenumber part is identical to the neutral limit from the stable side, and the low-wavenumber part has the form similar to that of Eq. (3). Therefore, we used a new fitting curve in order to determine the peak frequency (n_{\max}) at lower frequencies (smaller wavenumber) and to describe the observed power spectrum in both the high- and low-frequency regions as expressed in Eq. (4). $n_{H_{\max}}$ is the spectral peak frequency for the neutral limit approached from the stable side, and n_{\max} is the peak in the low frequency region, which is related to z_i that we want to determine from the fitting. A_H and A_L are curve fit coefficients. The best fit was achieved when B_L of the model was

Estimating the atmospheric boundary layer height over sloped

W. Choi et al.

Title Page

Abstract

Introduction

Conclusions

References

Tables

Figures



Back

Close

Full Screen / Esc

Printer-friendly Version

Interactive Discussion



set to 1.5, $A_H = 0.8$, and $n_{H_{\max}} = 0.16$ (Panofsky and Dutton, 1984) which described the observed spectra in both the CBL and under stable conditions above the canopy at Blodgett Forest. The example of the observed power spectrum of cross-wind velocity, Hojstrup's model modified by Panofsky and Dutton (1984), and the curve obtained by fitting Eq. (4) are shown in Fig. 3b.

$$\frac{nS(n)}{\sigma^2} = \frac{A_L(n/n_{\max})}{1 + B_L(n/n_{\max})^r} + \frac{A_H(n/n_{H_{\max}})}{1 + 1.5(n/n_{H_{\max}})^r} \quad (4)$$

Another method of estimating z_i involves the integral length scale (Λ) which can be derived from integral time scales using Taylor's frozen turbulence hypothesis as shown in Eq. (5) (Kaimal and Finnigan, 1994),

$$\Lambda_\alpha = \frac{\bar{U}}{\sigma_\alpha^2} \cdot \int_0^\infty R_\alpha(t) dt = \bar{U} \cdot \int_0^\infty \rho_\alpha(t) dt \quad (5)$$

$$R_\alpha(t) = \overline{\alpha'(x)\alpha'(x+t)} \quad (6)$$

where \bar{U} is the mean wind speed in the mean wind direction, σ_α^2 is the variance of variable α , $R_\alpha(t)$ is the auto-covariance function in time (Eq. 6), and $\rho_\alpha(t)$ is the auto-correlation function, that is the normalized auto-covariance function. In this study, the integral length scales of the horizontal winds were determined as the maxima of the integrals of $R_u(r)$ or $R_v(r)$ as shown in Fig. 4 (Lenschow and Stankov, 1986).

3.3 Power spectrum and integral length scale of lateral and longitudinal winds in Blodgett Forest

Vertical velocity spectra are known to obey Monin-Obukhov scaling at all wavelengths in the surface layer, depending on $n = f \cdot z/U$ and z/L (Panofsky and Dutton, 1984). Although Kaimal et al. (1982) suggested an empirical relationship between the peak

Estimating the atmospheric boundary layer height over sloped

W. Choi et al.

Title Page

Abstract

Introduction

Conclusions

References

Tables

Figures

⏪

⏩

◀

▶

Back

Close

Full Screen / Esc

Printer-friendly Version

Interactive Discussion



wavelength (λ_m) for vertical velocity and z_j , it is limited to the region above the surface layer ($0.1z_j \leq z \leq z_j$). Therefore, vertical velocity was not considered in this study.

Unlike results from towers over open and flat terrain or aircraft measurements (Lenschow and Stankov, 1986; Liu and Ohtaki, 1997; Kaimal and Finnigan, 1994), we found the lateral (v -) and longitudinal (u -) winds to exhibit significant differences both in the spectral and autocorrelation analyses above the canopy of Blodgett Forest, particularly in the unstable CBL. The power spectra and integral length scales of the lateral winds showed similar patterns under unstable conditions to those found in previous studies, in that (1) the shape of the power spectra under very slightly unstable conditions is similar to that of the neutral limit of stable air proposed by Panofsky and Dutton (1984) and Kaimal and Finnigan (1994), and (2) the spectral density at lower frequencies is augmented in the CBL, accompanying an increase in the integral length scale. On the other hand, the lower frequency part of the power spectrum for the longitudinal winds does not change much both in spectral density and the frequency of the spectral peak, showing nearly identical patterns to the neutral spectrum obtained in the early morning (Fig. 5). One possible explanation for the difference is that the horizontal wind, and specifically the longitudinal component, behaves differently over forested environments. Large eddies lying in the low frequency part of the spectrum adjust slowly to changing terrain unlike the high-frequency eddies, resulting in changes in spectral shapes. Britter et al. (1981) reported that the energy in higher frequency regions remains the same as over uniform terrain, but lower frequency energy decreases, particularly affecting the frequency of the longitudinal velocity component in mountainous terrain, similar to the observations over Blodgett Forest. Panofsky and Dutton (1984) explained that this is presumably due to divergence of horizontal wind (dU/dx) in the upslope motions, which dampens eddy vorticity, and “smears out” the structure of the largest eddies. Whatever the cause, we observed poor correlations of Λ and λ_m with z_j for the u -component winds, and hence we only consider the cross-wind v -component in the following analysis.

Estimating the atmospheric boundary layer height over sloped

W. Choi et al.

Title Page

Abstract

Introduction

Conclusions

References

Tables

Figures



Back

Close

Full Screen / Esc

Printer-friendly Version

Interactive Discussion



4 Comparisons of Λ and n_{\max} with z_i over the canopy of Blodgett Forest under unstable conditions

A 1:1 comparison between Λ_v and observed z_i both for 2007 and 2009 measurements is shown in Fig. 6a. Excluding four data points with unexpectedly deviated integral length scale values (18 August 11:30 ~ 13:00, 19 August 11:00 ~ 13:30, 20 August 08:30 ~ 10:00 in 2007, and 8 July 17:55 in 2009), which are marked by white and black dots, Λ_v exhibits a reasonable correlation with z_i ($R^2 = 0.55$ for 2007 and $R^2 = 0.43$ both for 2007 and 2009 measurements). The autocorrelation function, in general, tends to rapidly decrease with lag distance (Fig. 4) from 1 at $r = 0$ to below zero and then fluctuates around zero, indicative of a random relationship. However the autocorrelation function for the exceptionally high Λ_v values (three data points for 2007 measurements), sharply decreased within a short lag and exhibited a long tail well above zero, possibly due to a secular trend in the time-series not being completely removed. Although z_i appeared to be quite high (~ 1300 m) at 17:55 of 8 July, 2009, the surface heat flux was measured to be negative, meaning that turbulent buoyancy production had ceased by then and the ABL was already in transition. Thus, we also excluded that data point of 2009 from the analysis. The linear fits were obtained by the least squares method and are shown in Table 2. Oncley et al. (2004) used the relationship, $\Lambda_u \approx \Lambda_v = 0.45 \cdot z_i$ to estimate z_i over flat and open snow cover at the South Pole under unstable conditions, which was suggested by Lenschow and Stankov (1986) based on aircraft measurements over the ocean and Eastern Colorado. The relationship obtained over the ponderosa pine forest in this study was found to be $\Lambda_v = 0.15 \cdot z_i$. In addition, Lenschow and Stankov (1986) reported ratios of Λ_u to Λ_v near unity. However, the ratio of integral length scale in our study ranged widely from near unity in the morning to ~ 0.3 ($1\sigma = 0.15$) in the afternoon during the period of the tether-sonde measurements, which is much smaller than the ratio of 2 predicted by Batchelor (1953) for isotropic turbulence.

Estimating the atmospheric boundary layer height over sloped

W. Choi et al.

Title Page

Abstract

Introduction

Conclusions

References

Tables

Figures



Back

Close

Full Screen / Esc

Printer-friendly Version

Interactive Discussion



**Estimating the
atmospheric
boundary layer
height over sloped**

W. Choi et al.

Title Page

Abstract

Introduction

Conclusions

References

Tables

Figures



Back

Close

Full Screen / Esc

Printer-friendly Version

Interactive Discussion



Normalized frequencies of ABL-filling eddies, determined both from Eqs. (3) and (4) ($n_{\max,1}$ and $n_{\max,2}$, respectively), also show good agreement with the corresponding observed z_i as shown in Table 2 and Fig. (6b, c). One data point collected at 17:55 of 8 July in 2009 was excluded from the analysis for the same reason explained above for both $n_{\max,1}$ and $n_{\max,2}$. The slope of the linear fits obtained from the least squares method for both Λ_v and n_{\max} are changed less than 7% when 2009 data are included in the analysis compared to the slope when only 2007 data are used, implying these relationships can generally be applied to estimate z_i at least during the summer season of both 2007 and 2009. It further bears mention that because the spectral maxima in these CBL are located at scales of approximately 1000 m, which corresponds to ~ 300 s for typical surface winds at Blodgett Forest, this type of analysis does not require the high rate performance of a sonic anemometer and could, in principle, be obtained with 1–10 s averaged data. Similar attempts were made by Contini et al. (2009) over flat-terrain in a coastal site of the Salentum peninsula, in Italy with a focus on longitudinal winds. These authors report that, among the methods they applied, the spectral method showed the best correlation (correlation coefficient = 0.90) with radiosonde results. However, it should be noted that their comparison includes both unstable and stable conditions that could lead to a better correlation providing more data points at both ends of boundary layer height range.

Based on the regression relationships obtained above, daytime z_i was calculated for the entire period of the BEARPEX study in 2007. A timeseries of estimated z_i and corresponding observations is plotted in Fig. 7a for unstable conditions (07:30 ~ 17:30) during the period spanning the tethersonde measurements. The estimates from Λ_v tend to result in higher values particularly in the morning compared to both the observations and the estimates from n_{\max} . Nonetheless, the mean diurnal patterns of all the estimates from Λ_v , $n_{\max,1}$, and $n_{\max,2}$ for the 6 day tethersonde measurement period describe the observations fairly well as shown in Fig. 7b. It also appears that both the fully developed CBL heights and their temporal evolution of diurnal growth and decay are captured by the spectral estimation techniques. The monthly mean diurnal

patterns of the estimated atmospheric boundary layer height are shown in Fig. 8. The mean z_i in unstable environments (10:00 ~ 16:00 PST) is 780 m in August and 640 m in September 2007. For June and July 2009, the estimated mean daytime z_i is 790 m and 800 m, respectively. The decrease in z_i in September is likely due to reduced surface heat flux caused by lower surface temperature (Table 3). The NBL height is assumed to be the average of the observations from 2009.

The growth rate of z_i can be estimated with a simple slab theory for the intrusion of the mixed layer into a stably stratified free troposphere above, with a constant inversion strength (Eq. 7), sometimes referred to as an encroachment model (Batchvarova and Gryning, 1991), and presented in Fig. 7b for comparison.

$$\frac{dz_i}{dt} = \frac{(1 + \alpha)Q_0}{\gamma_\theta \rho C_p z_i} \quad (7)$$

Assuming an entrainment heat flux of 20% (α) of the surface heat flux (Q_0), γ_θ is the free tropospheric lapse rate above the boundary layer, and ρ and C_p are the density and specific heat capacity of air, respectively. With the calculated growth rate of the boundary layer (dz_i/dt) based on the observations of Q_0 and γ_θ , the boundary layer height at time t was calculated with 1-h time-step, assuming Q_0 and γ_θ are constant for 1 h. The initial z_i was set as the mean observed z_i for 08:00 ~ 09:00. The model results are presented in a gray solid line of Fig. 7b. The encroachment model fairly describes the growth of z_i through the late morning but fails to reproduce the fully developed boundary layer heights at this mountainous site. Although other z_i growth rate models, dealing with mechanical production of turbulence as well as the enthalpy budget, have been developed as summarized by Seibert et al. (2000), most need γ_θ and the initial condition of z_i to calculate boundary layer heights. In addition, the coefficients in the equations given in the literature differ considerably (Seibert et al., 2000). These limitations prevent routine estimation of z_i with surface measurements, which lends importance to the results of this study. We consider a discussion of the various z_i growth models to be beyond the scope of this work, all of which would necessarily neglect the

Estimating the atmospheric boundary layer height over sloped

W. Choi et al.

Title Page

Abstract

Introduction

Conclusions

References

Tables

Figures

⏪

⏩

◀

▶

Back

Close

Full Screen / Esc

Printer-friendly Version

Interactive Discussion



mesoscale subsidence above the ABL which we suspect is one of the principal causes for the relatively shallow boundary layers observed at Blodgett Forest.

5 Boundary layer heights (h) and power spectra of lateral winds in the stable nocturnal boundary layer (NBL)

5 During the BEARPEX 2009 campaign (15 June ~ 30 July, 2009), observed nocturnal boundary layer heights (h) ranged from 55 ~ 80 m (average of 67 ± 7 m), contained a strong above canopy inversion, and tended to be in steady-state throughout the night (Table 4). In general, the surface friction velocity and mean wind speed measured at the top of the observation tower (12.5 m a.g.l.) were relatively small (0.11 and 0.94 m s^{-1} , respectively) compared to those in the daytime for the period of radiosonde measurements (0.52 and 1.74 m s^{-1} , respectively). The relationships obtained for unstable conditions during the daytime (Table 2) were not able to successfully predict h mainly due to the differences in characteristics of turbulence between the NBL and CBL. In addition, both Λ and n_{max} did not show any correlation with h . Similar difficulties in the determination of spectral maxima were encountered by Contini et al. (2009), although they selected the maximum frequencies manually. In their study these difficulties were attributed to the interferences by external intermittency and non-turbulent phenomena such as meandering or wavy motions that produce non-stationarity (Contini et al., 2009).

20 Figure 9 shows four different types of power spectra for the crosswind component and temperature during the period of radiosonde measurements (Table 4). Power spectra for lateral winds in general show conformity in shape and spectral peak frequency with those for temperature in all cases. In group I and II (Fig. 9a, b), the maximum spectral density appears between $0.1 \sim 1$ of normalized frequency with lower densities in the lower frequency region, similar to typical spectral shapes of the neutral limit of the stable surface layer. Conversely, the density of the v -component winds in lower frequencies of group III and IV (Fig. 9c, d) tends to keep increasing. In addition, the

Estimating the atmospheric boundary layer height over sloped

W. Choi et al.

Title Page

Abstract

Introduction

Conclusions

References

Tables

Figures



Back

Close

Full Screen / Esc

Printer-friendly Version

Interactive Discussion



the NBL (Wu and Zhang, 2008; Zilitinkevich et al., 2009). Chemel et al. (2009) show that internal gravity waves are generated by the katabatic flow over an alpine valley with a period of ~ 7 min from their model results. Considering that the predominant wind at Blodgett Forest is a mesoscale mountain-valley wind system, internal gravity waves at the site are likely to be produced by the katabatic flow and could play an important role in mixing within the NBL when turbulence is weak. However, the origin and characteristics of the internal gravity waves are beyond the scope of this study. Enhanced spectral density in the lower frequency region shown in groups III and IV seems to be caused by other mesoscale motions rather than internal gravity waves.

$$h = a_1 u_* / f \quad (9)$$

$$h = a_2 \sqrt{u_* L} / f \quad (10)$$

$$h = a_3 u_* / N_{BV} \quad (11)$$

$$\frac{1}{h^2} = \frac{f^2}{(C_R u_*)^2} + \frac{N_{BV} f}{(C_{CN} u_*)^2} + \frac{f}{(C_{NS}^2 \kappa u_* L)} \quad (12)$$

Previous studies have suggested that nocturnal boundary layer heights (h) can be scaled with a combination of surface friction velocity (u_*), Obukhov length (L), Brunt-Väisälä frequency (N_{BV}) above the NBL, and/or the Coriolis parameter (f) as expressed in Eqs. (9) ~ (11) (Caughey et al., 1979; Kitaigorodskii and Joffre, 1988; Seibert et al., 2000; Zilitinkevich, 1972; Zilitinkevich et al., 2007). However, the constants $a_1 \sim a_3$ vary significantly in the literature with $a_1 = 0.07 \sim 0.3$, $a_2 = 0.3 \sim 0.7$, and $a_3 = 4 \sim 14$ (Caughey et al., 1979; Seibert et al., 2000). The direct comparisons between h and all corresponding parameters expressed in Eqs. (9) ~ (11) showed poor correlations with the fixed values of coefficients $a_1 \sim a_3$ (linear correlation coefficient, $r_1 = 0.25$ between h and u_*/f , $r_2 = 0.01$ for h vs. $\sqrt{u_* L}/f$, and $r_3 = 0.10$ for h and u_*/N_{BV}). Because observed h varied within a narrow range ($1\sigma = 7$ m) during the measurement period,

Estimating the atmospheric boundary layer height over sloped

W. Choi et al.

Title Page

Abstract

Introduction

Conclusions

References

Tables

Figures

⏪

⏩

◀

▶

Back

Close

Full Screen / Esc

Printer-friendly Version

Interactive Discussion



Estimating the atmospheric boundary layer height over sloped

W. Choi et al.

Title Page

Abstract

Introduction

Conclusions

References

Tables

Figures

⏪

⏩

◀

▶

Back

Close

Full Screen / Esc

Printer-friendly Version

Interactive Discussion



night. Wind direction varies clockwise (veering) with height from 1000 m to 3000 m, and the wind speed increases. Such variations in the geostrophic wind implies a baroclinic lower troposphere, in which air density depends on both temperature and pressure (i.e. the isotherms are not parallel to the pressure field) (Fig. 13). In such an atmosphere, the veering geostrophic winds result in warm air advection, enhancing the stability of the layer (Holton, 2004). This vertical shear of the geostrophic wind is called the thermal wind because it is a consequence of the horizontal temperature gradient (Holton, 2004), in this case the result of intense surface heating of the Mojave/Sonoran desert region. The difference in the geostrophic wind speeds can be estimated by Eq. (13), where V_g is the geostrophic wind, R is gas constant for dry air, f is Coriolis parameter, p is pressure, and $\nabla_p T$ is temperature gradient on an isobaric surface:

$$\begin{aligned}
 V_g(p_1) - V_g(p_0) &= \frac{R_d}{f} \nabla_p T \cdot \ln \left(\frac{p_0}{p_1} \right) \\
 &= \left(\frac{287 \text{ J kg}^{-1} \text{ K}^{-1}}{9.2 \times 10^{-5} \text{ s}^{-1}} \right) \left(\frac{1 \text{ K}}{158 \text{ km}} \right) \ln \left(\frac{700 \text{ mb}}{600 \text{ mb}} \right) = 3.0 \text{ m s}^{-1}
 \end{aligned}
 \tag{13}$$

Equation (13) yields a change in the geostrophic wind speed (thermal wind) of 3.1 m s^{-1} between 1500 ~ 3000 m, using the observed mean temperature gradient (NOAA, 2010) at 700 mbar height for the whole BEAPREX period in 2009. This calculation is roughly consistent with the observed winds aloft at Blodgett Forest (Fig. 13). Such a high shear layer near the ABL top could enhance entrainment by producing mechanical turbulent kinetic energy. In addition, consistent southerlies or southwesterlies aloft likely provide air that is heavily influenced by anthropogenic sources from the southern Central Valley of California.

7 Concluding remarks

In this study estimates of atmospheric boundary layer height (z_i) using the peak frequency in the low-frequency region of the power spectrum of lateral winds and the integral length scales obtained from sonic anemometry, are presented. The estimates based on surface tower data show reasonably good agreement with observations under unstable conditions over a ponderosa pine forest located on the western slope of the Sierra-Nevada.

In stable NBL environments, the power spectrum of horizontal winds was strongly influenced by internal gravity waves and/or mesoscale mountainous air motions, showing the conformity of peak spectral frequency both with Brunt-Väisälä frequency and the peak frequency of the temperature spectrum. Although the NBL height was not able to be estimated from spectral analysis due to interference by dynamics other than turbulence, observed NBL heights were fairly consistent with the mean of 67 m ($1\sigma = \pm 7$ m) regardless of time of night. The simple diagnostic equations for scaling h with measurable parameters, such as friction velocity (u_*), the mean wind speed (\bar{U}), the Obukhov length (L), Coriolis parameter (f), and Brunt-Väisälä frequency (N_{BV}) above the NBL, was also used. Among several diagnostic equations examined in this study, only the equation suggested by Zilitinkevich et al. (2007) showed a reasonable agreement with observations. However, the limited data available and limited variation in observed h give rise to the need for further studies in order to draw any definite conclusions.

Based on the relationships for unstable air obtained from spectral analyses during BEARPEX 2007 and the observations of the NBL height in BEARPEX 2009, the monthly mean diurnal patterns of the estimated atmospheric boundary layer height are presented in Fig. 8. The estimated mean z_i in the CBL environments (10:00 ~ 16:00 PST) is 780 m (median 810 m) in August and 640 m (median 660 m) in September 2007. The monthly variations in the fully developed CBL depths most likely resulted from the variations in solar radiation intensities and hence in the surface heat flux.

Estimating the atmospheric boundary layer height over sloped

W. Choi et al.

Title Page

Abstract

Introduction

Conclusions

References

Tables

Figures



Back

Close

Full Screen / Esc

Printer-friendly Version

Interactive Discussion



Estimating the atmospheric boundary layer height over sloped

W. Choi et al.

Title Page

Abstract

Introduction

Conclusions

References

Tables

Figures

⏪

⏩

◀

▶

Back

Close

Full Screen / Esc

Printer-friendly Version

Interactive Discussion



- Britter, R. E., Hunt, J. C. R., and Richards, K. J.: Air-flow over a two-dimensional hill – studies of velocity speed-up, roughness effects and turbulence, *Q. J. R. Meteor. Soc.*, 107, 91–110, 1981.
- Burk, S. D. and Thompson, W. T.: The summertime low-level jet and marine boundary layer structure along the California coast, *Mon. Weather Rev.*, 124, 668–686, 1996.
- Caughey, S. J., Wyngaard, J. C., and Kaimal, J. C.: Turbulence in the evolving stable boundary-layer, *J. Atmos. Sci.*, 36, 1041–1052, 1979.
- Chemel, C., Staquet, C., and Largeron, Y.: Generation of internal gravity waves by a katabatic wind in an idealized alpine valley, *Meteorol. Atmos. Phys.*, 103, 187–194, 2009.
- Contini, D., Cava, D., Martano, P., Donato, A., and Grasso, F. M.: Comparison of indirect methods for the estimation of boundary layer height over flat-terrain in a coastal site, *Meteorol. Z.*, 18(3), 309–320, 2009.
- Day, D. A., Wooldridge, P. J., and Cohen, R. C.: Observations of the effects of temperature on atmospheric HNO₃, ΣANs, ΣPNs, and NO_x: evidence for a temperature-dependent HO_x source, *Atmos. Chem. Phys.*, 8, 1867–1879, doi:10.5194/acp-8-1867-2008, 2008.
- Dillon, M. B., Lamanna, M. S., Schade, G. W., Goldstein, A. H., and Cohen, R. C.: Chemical evolution of the Sacramento urban plume: Transport and oxidation, *J. Geophys. Res.-Atmos.*, 107, 4045, doi:10.1029/2001jd000969, 2002.
- Goldstein, A. H., Hultman, N. E., Fracheboud, J. M., Bauer, M. R., Panek, J. A., Xu, M., Qi, Y., Guenther, A. B., and Baugh, W.: Effects of climate variability on the carbon dioxide, water, and sensible heat fluxes above a ponderosa pine plantation in the Sierra Nevada (CA), *Agr. Forest Meteorol.*, 101, 113–129, 2000.
- Hanna, S. R.: Thickness of planetary boundary layer, *Atmos. Environ.*, 3, 519–536, 1969.
- Hojstrup, J.: Velocity spectra in the unstable planetary boundary-layer, *J. Atmos. Sci.*, 39, 2239–2248, 1982.
- Holton, J. R.: *An Introduction to Dynamic Meteorology* 4th edition, Elsevier Academic Press, Burlington, 2004.
- Holzworth: Estimates of mean maximum mixing depths in the contiguous United States, *Mon. Weather Rev.*, 92, 235–242, 1964.
- Kaimal, J. C.: Horizontal velocity spectra in an unstable surface-layer, *J. Atmos. Sci.*, 35, 18–24, 1978.
- Kaimal, J. C., Abshire, N. L., Chadwick, R. B., Decker, M. T., Hooke, W. H., Kropfli, R. A., Neff, W. D., and Pasqualucci, F.: Estimating the depth of the daytime convective boundary-layer,

Estimating the atmospheric boundary layer height over sloped

W. Choi et al.

Title Page

Abstract

Introduction

Conclusions

References

Tables

Figures

⏪

⏩

◀

▶

Back

Close

Full Screen / Esc

Printer-friendly Version

Interactive Discussion



J. Appl. Meteorol., 21, 1123–1129, 1982.

Kaimal, J. C. and Finnigan, J. J.: Atmospheric Boundary Layer Flows: Their Structure and Measurement, Oxford University Press, 1994.

Kitaigorodskii, S. A. and Joffre, S. M.: In search of a simple scaling for the height of the stratified atmospheric boundary layer, Tellus A, 40A, 419–433, 1988.

Kossmann, M., Vogtlin, R., Corsmeier, U., Vogel, B., Fiedler, F., Binder, H. J., Kalthoff, N., and Beyrich, F.: Aspects of the convective boundary layer structure over complex terrain, Atmos. Environ., 32, 1323–1348, 1998.

Lenschow, D. H. and Stankov, B. B.: Length scales in the convective boundary-layer, J. Atmos. Sci., 43, 1198–1209, 1986.

Liu, X. H. and Ohtaki, E.: An independent method to determine the height of the mixed layer, Bound.-Lay. Meteorol., 85, 497–504, 1997.

McNider, R. T.: A note on velocity fluctuations in drainage flows, J. Atmos. Sci., 39, 1658–1660, 1982.

Misson, L., Tang, J. W., Xu, M., McKay, M., and Goldstein, A.: Influences of recovery from clear-cut, climate variability, and thinning on the carbon balance of a young ponderosa pine plantation, Agr. Forest Meteorol., 130, 207–222, doi:10.1016/j.agrformet.2005.04.001, 2005. NOAA (Earth System Research Laboratory), available at: <http://www.esrl.noaa.gov/psd/cgi-bin/data/composites/printpage.pl>, 2010.

Oncley, S. P., Buhr, M., Lenschow, D. H., Davis, D., and Semmer, S. R.: Observations of summertime NO fluxes and boundary-layer height at the South Pole during ISCAT 2000 using scalar similarity, Atmos. Environ., 38, 5389–5398, doi:10.1016/j.atmosenv.2004.05.053, 2004.

Panofsky, H. A., Tennekes, H., Lenschow, D. H., and Wyngaard, J. C.: The characteristics of turbulent velocity components in the surface layer under convective conditions, Bound.-Lay. Meteorol., 11, 355–361, 1977.

Panofsky, H. A. and Dutton, J. A.: Atmospheric Turbulence: Models and Methods for Engineering Applications, John Wiley & Sons, Inc., 1984.

Seaman, N. L., Stauffer, D. R., and Lariogibbs, A. M.: A multiscale 4-dimensional data assimilation system applied in the San-Joaquin valley during sarmap .1. Modeling design and basic performance-characteristics, J. Appl. Meteorol., 34, 1739–1761, 1995.

Seibert, P., Beyrich, F., Gryning, S. E., Joffre, S., Rasmussen, A., and Tercier, P.: Review and intercomparison of operational methods for the determination of the mixing height, Atmos.

Estimating the atmospheric boundary layer height over sloped

W. Choi et al.

Title Page

Abstract

Introduction

Conclusions

References

Tables

Figures

⏪

⏩

◀

▶

Back

Close

Full Screen / Esc

Printer-friendly Version

Interactive Discussion



Environ., 34, 1001–1027, 2000.

Stull, R. B.: An Introduction to Boundary Layer Meteorology, Kluwer Academic Publishers, 1988.

Sullivan, P. P., Moeng, C. H., Stevens, B., Lenschow, D. H., and Mayor, S. D.: Structure of the entrainment zone capping the convective atmospheric boundary layer, *J. Atmos. Sci.*, 55, 3042–3064, 1998.

Taylor, G. I.: The spectrum of turbulence, *Proc. Roy. Soc. A*, 164, 476–490, 1938.

Wu, X. and Zhang, J.: Instability of a stratified boundary layer and its coupling with internal gravity waves, Part 1. Linear and nonlinear instabilities, *J. Fluid Mech.*, 595, 379–408, 2008.

Wyngaard, J. C. and Lemone, M. A.: Behavior of the refractive-index structure parameter in the entraining convective boundary-layer, *J. Atmos. Sci.*, 37, 1573–1585, 1980.

Wyngaard, J. C.: Structure of the PBL in Lectures on air pollution modeling, edited by: Venkatram, A. and Wyngaard, J. C., American Meteorological Society, Boston, 1988.

Wyngaard, J. C.: Turbulence in the atmosphere, Cambridge University Press, Cambridge, 2010.

Zeng, X. B., Brunke, M. A., Zhou, M. Y., Fairall, C., Bond, N. A., and Lenschow, D. H.: Marine atmospheric boundary layer height over the eastern Pacific: Data analysis and model evaluation, *J. Climate*, 17, 4159–4170, 2004.

Zilitinkevich, S., Esau, I., and Baklanov, A.: Further comments on the equilibrium height of neutral and stable planetary boundary layers, *Q. J. R. Meteor. Soc.*, 133, 265–271, doi:10.1002/qj.27, 2007.

Zilitinkevich, S. S.: On the determination of the height of the Ekman boundary layer, *Bound.-Lay. Meteorol.*, 3, 141–145, 1972.

Zilitinkevich, S. S., Elperin, T., Kleorin, N., L'Vov, V., and Rogachevskii, I.: Energy- and Flux-Budget Turbulence Closure Model for Stably Stratified Flows. Part II: The Role of Internal Gravity Waves, *Bound.-Lay. Meteorol.*, 133, 139–164, doi:10.1007/s10546-009-9424-0, 2009.

Table 1. Time of sonde flight, measurements conducted during flights, observed z_i , z_d/L , u_* , and U obtained from the tower at 12.5 m a.g.l.

Date	Time (PST)	Measurements	z_i (m)	$-z_d/L$	u_*	\bar{U}
18 August 2007	10:10 ~ 10:41 ^a		800	0.072	0.71	2.70
	12:00 ~ 12:25 ^b		800	0.097	0.74	2.30
	12:25 ~ 12:52 ^a		950	0.094	0.71	2.51
	14:06 ~ 14:28 ^b		850	0.095	0.71	2.40
	14:28 ~ 14:49 ^a		950	0.083	0.71	2.41
	15:55 ~ 16:15 ^b		800	0.071	0.58	2.12
	08:18 ~ 08:42 ^a		325	0.037	0.61	2.77
19 August 2007	09:55 ~ 10:19 ^b		465	0.060	0.73	2.86
	10:19 ~ 10:38 ^a		625	0.064	0.74	2.96
	11:29 ~ 11:52 ^b	pressure, temperature,	700	0.048	0.84	3.40
	13:35 ~ 14:03 ^a	RH, wind speed,	850	0.057	0.82	3.16
	15:12 ~ 15:38 ^b	wind direction	800	0.068	0.68	2.58
	09:05 ~ 09:37 ^a		450	0.092	0.53	2.20
	10:38 ~ 11:18 ^b		650	0.111	0.61	2.50
20 August 2007	11:18 ~ 11:36 ^a		850	0.134	0.57	2.40
	12:49 ~ 13:17 ^b		800	0.186	0.58	1.83
	14:55 ~ 15:22 ^a		625	0.137	0.55	2.14
	16:36 ~ 16:56 ^b		650	0.119	0.43	1.65
21 August 2007	08:35 ~ 09:13 ^a		200	0.313	0.32	0.80
	10:23 ~ 10:51 ^b		780	0.162	0.57	1.95
	09:30 ~ 09:59 ^a		600	0.303	0.43	1.27
23 August 2007	11:37 ~ 12:04 ^b	pressure, temperature,	550	0.227	0.52	1.93
	12:04 ~ 12:20 ^a	RH	600	0.221	0.55	1.99
25 June 2009	13:49 ^c		920	0.134	0.60	1.83
8 July 2009	17:55 ^c		1200	-0.008	0.39	1.48
9 July 2009	10:12 ^c	altitude, temperature,	1000	0.063	0.68	2.25
9 July 2009	16:38 ^c	RH, wind speed,	1100	0.070	0.47	1.52
21 July 2009	16:16 ^c	wind direction	700	0.062	0.46	1.45
22 July 2009	12:25 ^c		600	0.091	0.59	1.90

^a ascending measurement.

^b descending measurement.

^c launching time.

Estimating the atmospheric boundary layer height over sloped

W. Choi et al.

Title Page

Abstract

Introduction

Conclusions

References

Tables

Figures

◀

▶

◀

▶

Back

Close

Full Screen / Esc

Printer-friendly Version

Interactive Discussion



Estimating the atmospheric boundary layer height over sloped

W. Choi et al.

Title Page

Abstract

Introduction

Conclusions

References

Tables

Figures

⏪

⏩

◀

▶

Back

Close

Full Screen / Esc

Printer-friendly Version

Interactive Discussion

Table 2. Correlation between observed z_i vs. integral length scale and normalized maximal spectral frequency.

	Linear fit (R^2)	
	2007 only	2007 and 2009
Integral length scale (Λ_v)	$\Lambda_v = 0.145z_i(0.55)$	$\Lambda_v = 0.141z_i(0.43)$
Max. spectral freq. ($n_{\max,1}$) from Eq. (3)	$1/n_{\max,1} = 6.98 \times 10^{-2} \cdot z_i(0.37)$	$1/n_{\max,1} = 6.92 \times 10^{-2} \cdot z_i(0.42)$
Max. spectral freq. ($n_{\max,2}$) from Eq. (4)	$1/n_{\max,2} = 1.52 \times 10^{-1} \cdot z_i(0.32)$	$1/n_{\max,2} = 1.66 \times 10^{-1} \cdot z_i(0.41)$

Estimating the atmospheric boundary layer height over sloped

W. Choi et al.

Title Page

Abstract

Introduction

Conclusions

References

Tables

Figures

⏪

⏩

◀

▶

Back

Close

Full Screen / Esc

Printer-friendly Version

Interactive Discussion



Table 3. Monthly mean, median, and standard deviation of estimated atmospheric boundary layer heights for unstable conditions (10:00 ~ 16:00) during the whole BEARPEX period both in 2007 and 2009.

	Estimated Boundary Layer Heights, z_i (m)			
	August (2007)	September (2007)	June (2009)	July (2009)
Mean	783	639	786	801
Median	758	583	711	707
1σ	299	295	371	375

Estimating the atmospheric boundary layer height over sloped

W. Choi et al.

Title Page

Abstract

Introduction

Conclusions

References

Tables

Figures

⏪

⏩

◀

▶

Back

Close

Full Screen / Esc

Printer-friendly Version

Interactive Discussion



Table 4. Radio sonde launching time, observed nocturnal boundary layer height (h), surface friction velocity (u_*), mean wind speed (\bar{U}) at z_d of 6 m, lapse rate of virtual potential temperature above h ($d(\ln\theta)/dz$), and Obukhov length (L). Nighttime spectra of lateral winds and temperature are grouped according to their shapes and peak spectral frequencies.

Flight time (PST)	h (m)	u_*	\bar{U}	$(d(\ln\theta)/dz)$ (m^{-1})	L	Spectral group
22 June 2009 23:00	65	0.09	0.33	2.53×10^{-5}	-4.7	I
23 June 2009 22:56	70	0.13	1.37	3.41×10^{-5}	12.3	I
23 June 2009 23:19	75	0.15	1.59	6.85×10^{-5}	13.5	I
25 June 2009 03:57	80	0.19	1.56	3.64×10^{-5}	20.8	II
9 July 2009 01:25	80	0.08	0.74	1.60×10^{-5}	101	III
14 July 2009 19:52	70	0.06	0.67	9.03×10^{-6}	-13.7	IV
15 July 2009 05:51	65	0.08	1.04	4.23×10^{-5}	-28.1	III
17 July 2009 00:53	65	0.16	0.89	5.14×10^{-5}	11.0	II
21 July 2009 21:41	55	0.05	0.96	9.50×10^{-7}	-231	IV
22 July 2009 02:41	60	0.10	0.69	2.79×10^{-5}	15.2	I
24 July 2009 23:55	80	0.05	0.45	1.12×10^{-5}	36.8	III
29 July 2009 07:17	65	0.23	1.05	3.13×10^{-5}	112	II
Mean (1σ)	67 (7)	0.11 (0.06)	0.96 (0.46)	2.95×10^{-5} (1.91×10^{-5})		

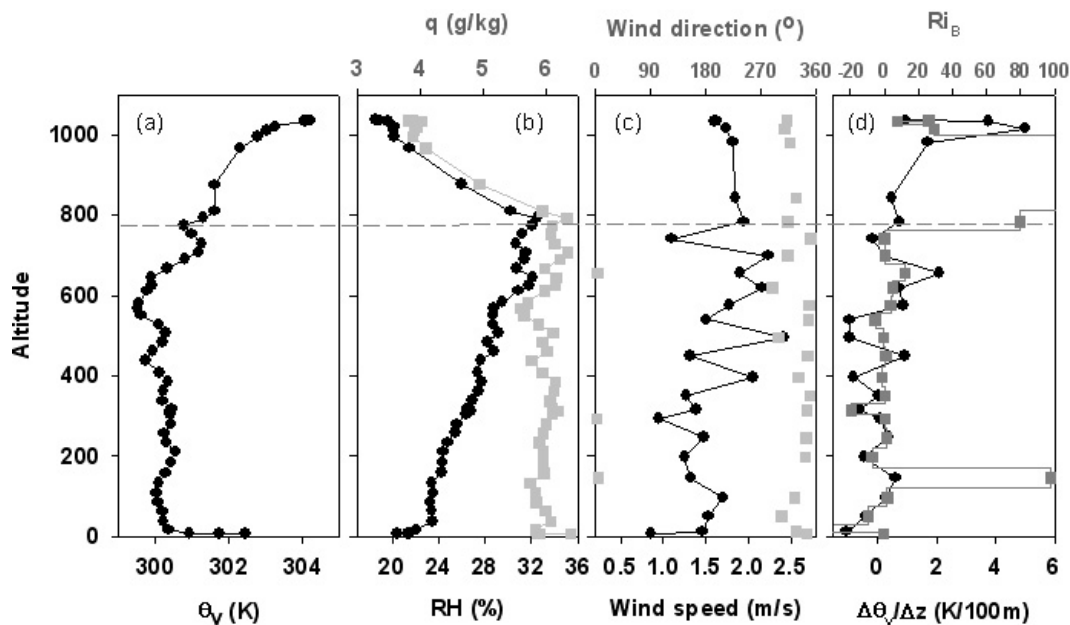


Fig. 1. Vertical profiles of **(a)** virtual potential temperature (θ_v), **(b)** specific (q) and relative (RH) humidity, **(c)** wind speed and direction, and **(d)** vertical gradient of θ_v and bulk Richardson number (Ri_b) for 10:23 ~ 10:51 of 21 August 2007. Data were obtained with balloon tether-sonde measurements. Horizontal dashed line represents boundary layer height (z_l).

Estimating the atmospheric boundary layer height over sloped

W. Choi et al.

Title Page

Abstract

Introduction

Conclusions

References

Tables

Figures

◀

▶

◀

▶

Back

Close

Full Screen / Esc

Printer-friendly Version

Interactive Discussion

Estimating the atmospheric boundary layer height over sloped

W. Choi et al.

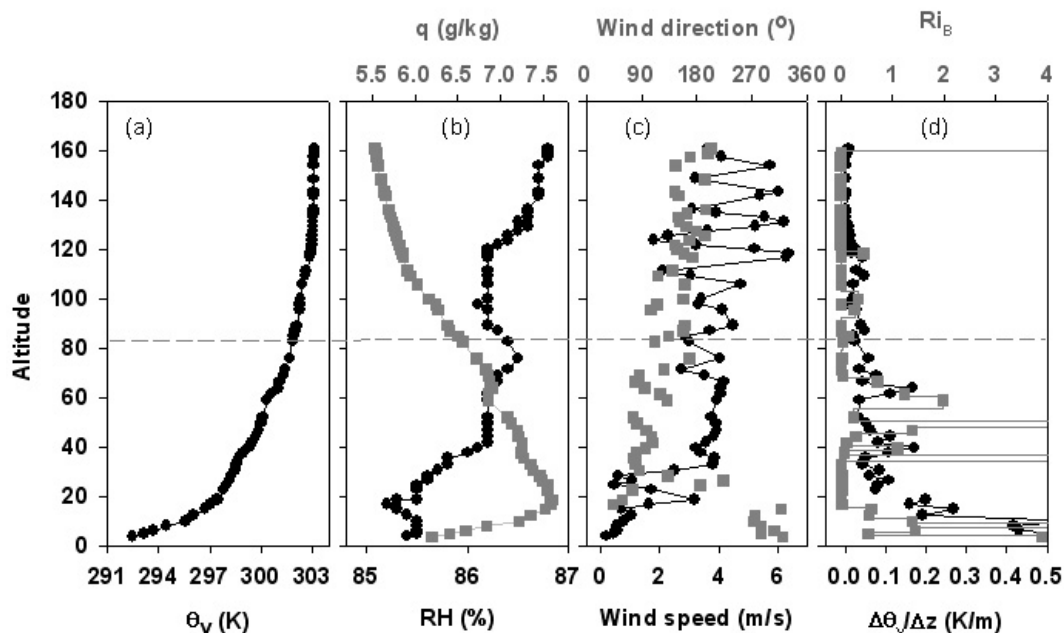


Fig. 2. Nighttime vertical profiles of **(a)** virtual potential temperature (θ_v), **(b)** specific (q) and relative (RH) humidity, **(c)** wind speed and direction, and **(d)** vertical gradient of θ_v and bulk Richardson number (Ri_b) for the radiosonde flight launched at 01:25 PST of 9 July 2009. Horizontal dashed line represents nocturnal boundary layer height (h).

Estimating the atmospheric boundary layer height over sloped

W. Choi et al.

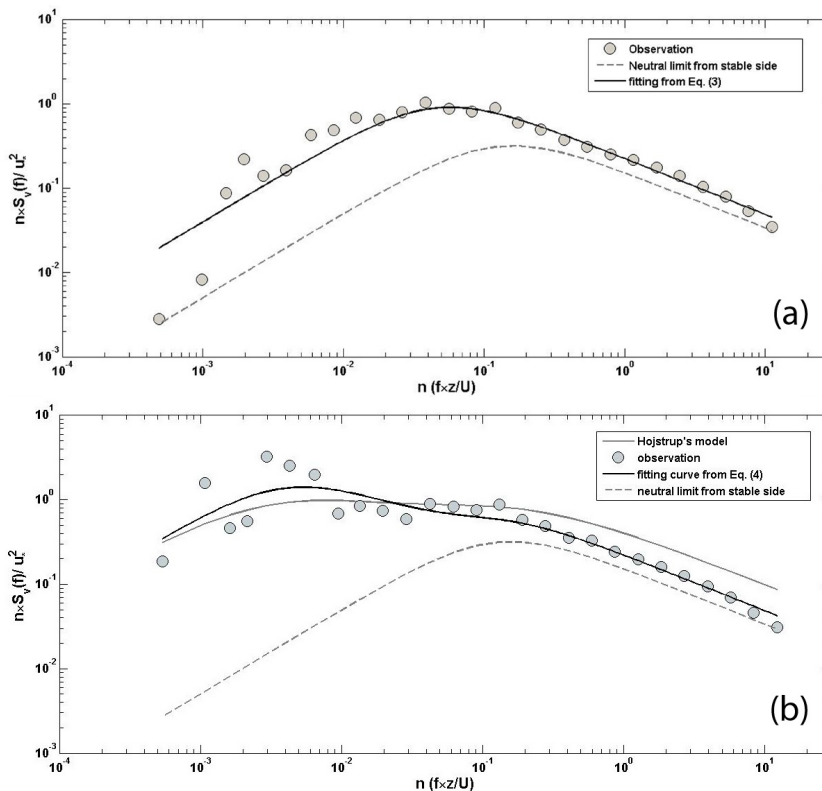


Fig. 3. Power spectrum of lateral winds obtained on 18 August 2007 for **(a)** slightly unstable air (07:30 ~ 09:00; $-z/L = 0.038$) and **(b)** CBL (12:00 ~ 13:30; $-z/L = 0.094$). Gray circles denote observation points, black solid lines represent fitting curves obtained from Eqs. (3) and (4), gray dashed lines describe the spectrum for neutral limit from stable side with $A_0 = 0.8$ and $n_{\max} = 0.16$, and gray solid line shows the result of Hojstrup's model with $L = -70.1$ and $z_i = 950$ m.

Title Page

Abstract

Introduction

Conclusions

References

Tables

Figures

◀

▶

◀

▶

Back

Close

Full Screen / Esc

Printer-friendly Version

Interactive Discussion



Estimating the atmospheric boundary layer height over sloped

W. Choi et al.

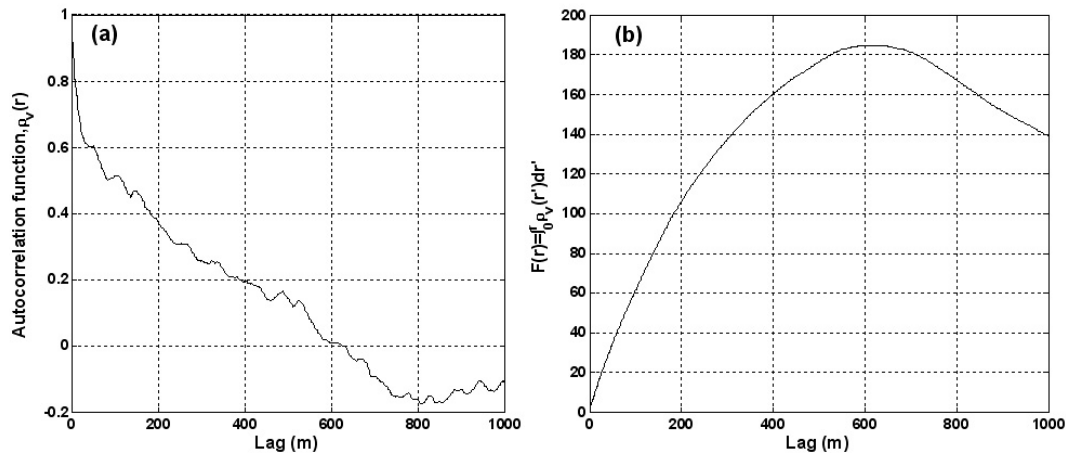


Fig. 4. Example (12:00 ~ 13:30 18 August 2007) of **(a)** autocorrelation of v -component and **(b)** corresponding integral of autocorrelation, $F(r) = \int_0^r \rho_v(r') dr'$ as a function of distance lag (m), which was derived assuming Taylor's frozen turbulence hypothesis. Integral length scale was taken as $F(r)$ at its first maximum.

Title Page

Abstract

Introduction

Conclusions

References

Tables

Figures

◀

▶

◀

▶

Back

Close

Full Screen / Esc

Printer-friendly Version

Interactive Discussion

Estimating the atmospheric boundary layer height over sloped

W. Choi et al.

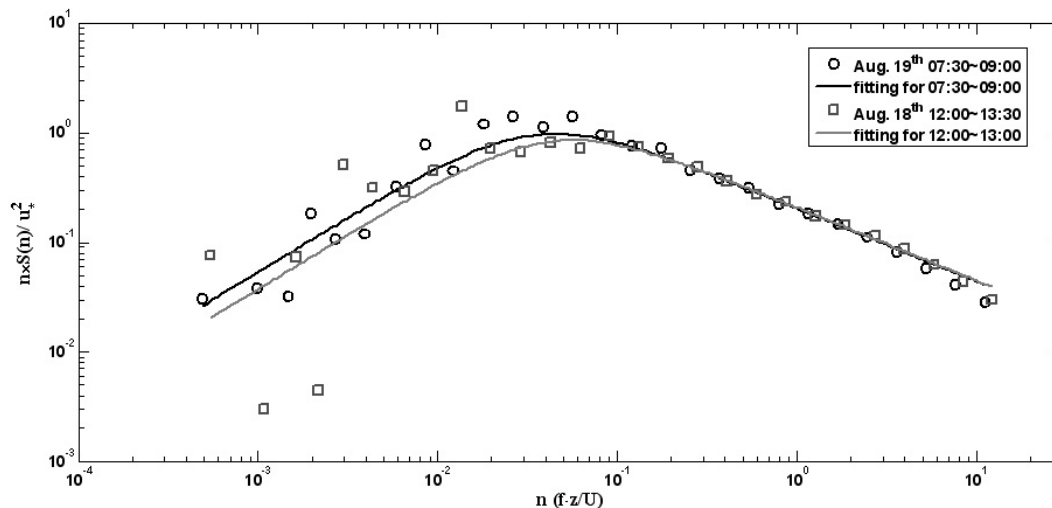


Fig. 5. Power spectra of longitudinal winds obtained under slightly unstable conditions (black circles; 07:30~09:00 on 19 August) and in fully developed boundary layer (gray squares; 12:00~13:30 on 18 August). Black and gray solid lines represent fitting curves for slightly unstable air and CBL, respectively.

Title Page

Abstract

Introduction

Conclusions

References

Tables

Figures

◀

▶

◀

▶

Back

Close

Full Screen / Esc

Printer-friendly Version

Interactive Discussion

Estimating the atmospheric boundary layer height over sloped

W. Choi et al.

Title Page

Abstract

Introduction

Conclusions

References

Tables

Figures

◀

▶

◀

▶

Back

Close

Full Screen / Esc

Printer-friendly Version

Interactive Discussion

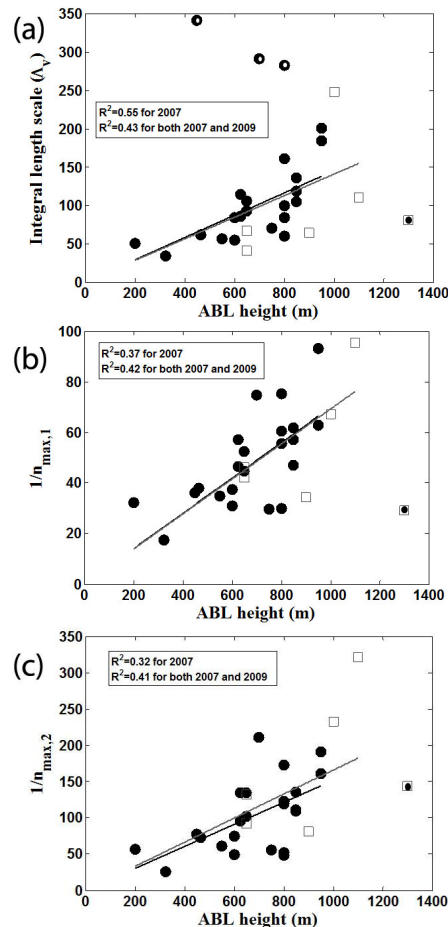


Fig. 6. The comparison of observed ABL height to (a) integral length scale (λ), (b) $1/n_{\max,1}$ and (c) $1/n_{\max,2}$ for the lateral (cross-stream) component (v) of the wind, where $n_{\max,1}$ and $n_{\max,2}$ are normalized spectral peak frequency obtained from Eqs. (3) and (4), respectively. Black circles represent data for BEARPEX 2007 and gray squares for 2009. Black lines denote the linear fit only for 2007 data and gray lines for the whole data points except those marked by black and white dots. Detailed results are also presented in Table 2.

Estimating the atmospheric boundary layer height over sloped

W. Choi et al.

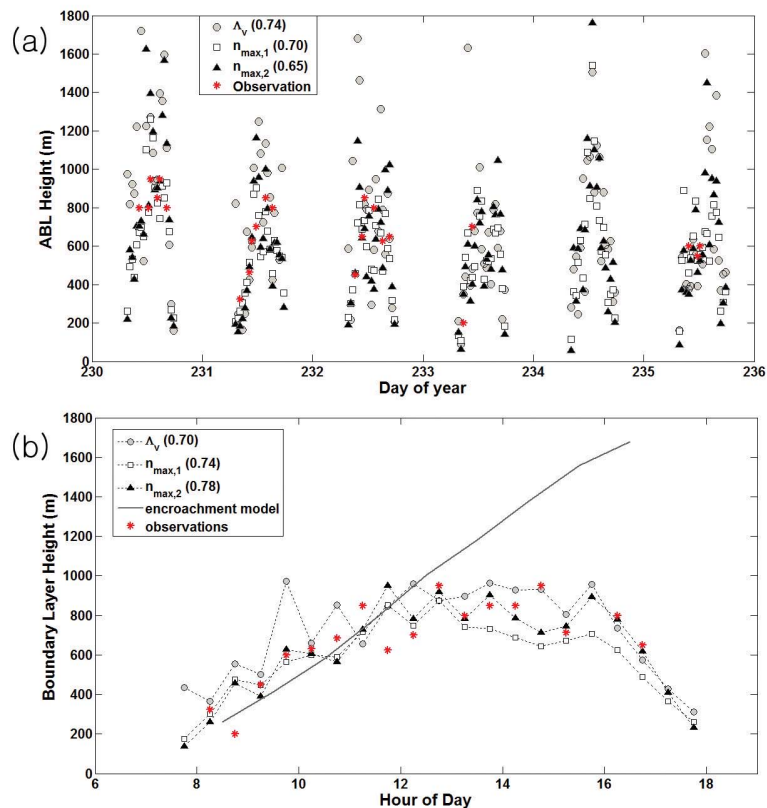


Fig. 7. (a) Time-series and (b) mean diurnal patterns of estimated z_i and corresponding observations during the tether sonde measurements from day 230 ~ 235 (18 August 2007 ~ 23 August 2007) for unstable conditions (07:30 ~ 17:30). Gray circles represent z_i estimates from Λ_V , white squares estimates from $n_{\max,1}$, and black triangles from $n_{\max,2}$. Red asterisks denote the observations and thick gray solid line represents the result of an encroachment model expressed in Eq. (7). The values in parentheses within the legend show the correlation coefficients between diurnally averaged estimates from each method and the observations.

Title Page

Abstract

Introduction

Conclusions

References

Tables

Figures

◀

▶

◀

▶

Back

Close

Full Screen / Esc

Printer-friendly Version

Interactive Discussion

Estimating the atmospheric boundary layer height over sloped

W. Choi et al.

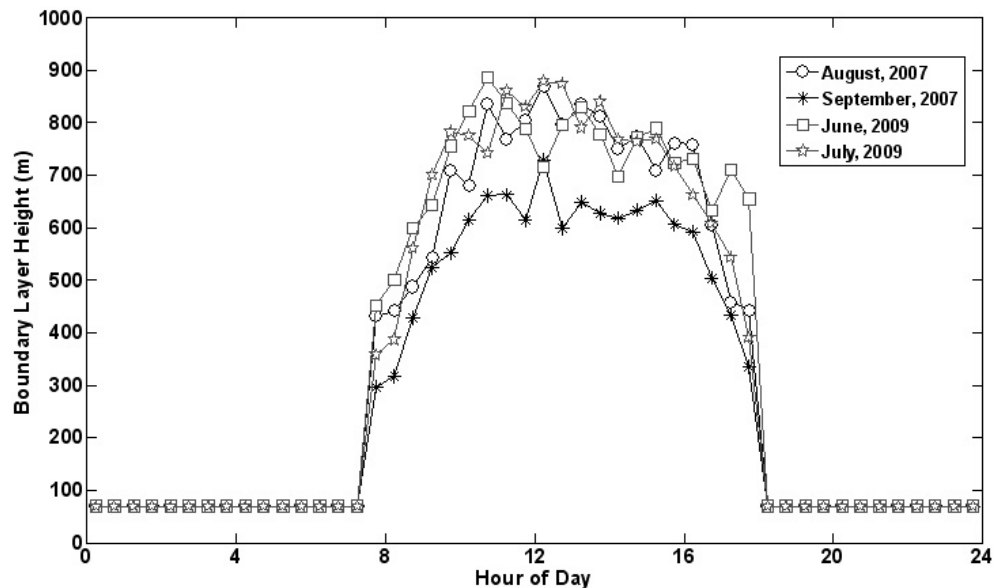


Fig. 8. Monthly mean diurnal patterns of estimated ABL heights during the BEARPEX 2007 and 2009 campaigns. The NBL height is the mean value (67 m) obtained from radiosonde measurements conducted during BEARPEX 2009. White circles and asterisks represent the monthly mean estimate of z_i for August and September in 2007, respectively, and white squares and stars for June and July in 2009.

[Title Page](#)
[Abstract](#)
[Introduction](#)
[Conclusions](#)
[References](#)
[Tables](#)
[Figures](#)
[◀](#)
[▶](#)
[◀](#)
[▶](#)
[Back](#)
[Close](#)
[Full Screen / Esc](#)
[Printer-friendly Version](#)
[Interactive Discussion](#)

Estimating the atmospheric boundary layer height over sloped

W. Choi et al.

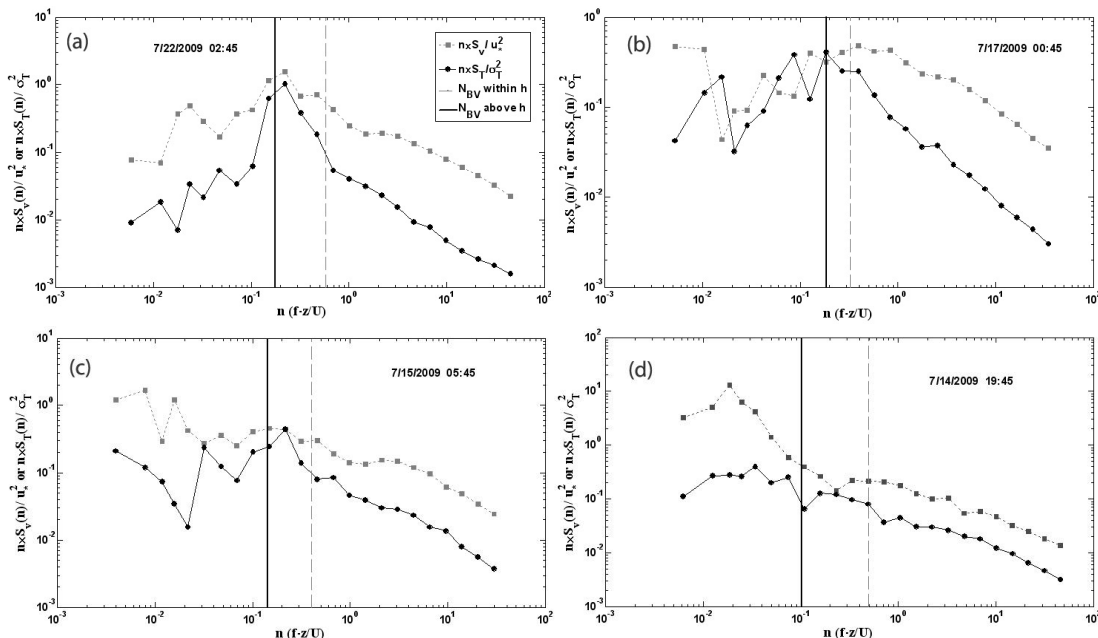


Fig. 9. Power spectra of lateral winds and temperature under NBL conditions during BEARPEX 2009. Black circles represent temperature power spectrum normalized by the variance of temperature and gray squares denote the power spectrum of lateral winds normalized by friction velocity. Black vertical line denotes Brunt-Väisälä frequency (N_{BV}) above the NBL and gray dashed line shows N_{BV} within the NBL. All spectra obtained in 2009 show four different patterns **(a)** group I, **(b)** group II, **(c)** group III, and **(d)** group IV according to spectrum shape and the position of peak spectral frequency as explained in text. In general, spectral peak of lateral winds tend to correspond to both the spectral peak of temperature.

Title Page

Abstract

Introduction

Conclusions

References

Tables

Figures

◀

▶

◀

▶

Back

Close

Full Screen / Esc

Printer-friendly Version

Interactive Discussion

Estimating the atmospheric boundary layer height over sloped

W. Choi et al.

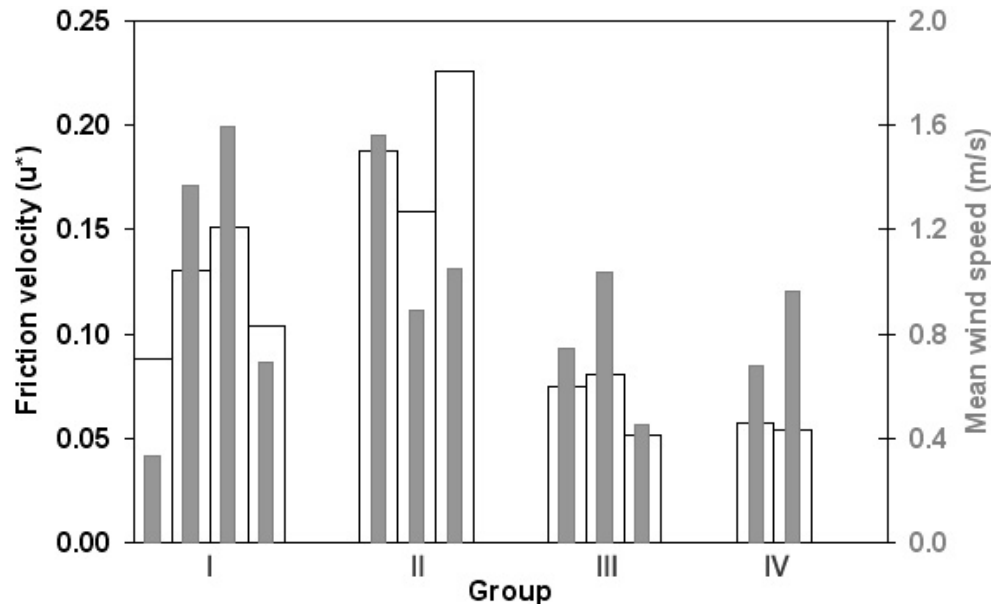


Fig. 10. Bar plot of friction velocity (u_*) and mean wind speed (\bar{U}) according to groups which are categorized based on the spectral shapes for lateral winds and temperature, and conformity with N_{BV} . Open white bars represent friction velocity and gray bars denote mean wind speed.

Title Page

Abstract

Introduction

Conclusions

References

Tables

Figures

◀

▶

◀

▶

Back

Close

Full Screen / Esc

Printer-friendly Version

Interactive Discussion



Estimating the atmospheric boundary layer height over sloped

W. Choi et al.

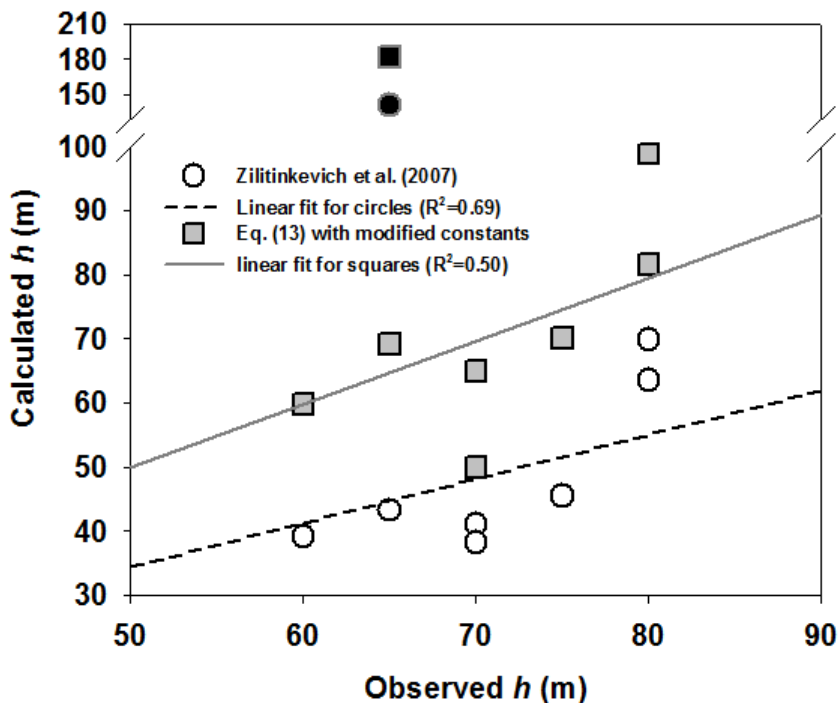


Fig. 11. Comparison of observed NBL heights (h) with calculated NBL height. Calculated h was obtained from Eq. (12) with CR = 0.6, CCN = 1.36, CNS = 0.51 (white circles) recommended by Zilitinkevich et al. (2007) and CR = 0.6, CCN = 1.25, CNS = 0.9 (gray squares) modified in this study. Black short-dashed line represents the best linear fits for white circles with the slope of 0.69 ($R^2 = 0.67$) and gray solid line for gray squares with the slope of 0.99 ($R^2 = 0.50$). Black square and circle were not included in linear fit calculations.

[Title Page](#)
[Abstract](#)
[Introduction](#)
[Conclusions](#)
[References](#)
[Tables](#)
[Figures](#)
[◀](#)
[▶](#)
[◀](#)
[▶](#)
[Back](#)
[Close](#)
[Full Screen / Esc](#)
[Printer-friendly Version](#)
[Interactive Discussion](#)

Estimating the atmospheric boundary layer height over sloped

W. Choi et al.

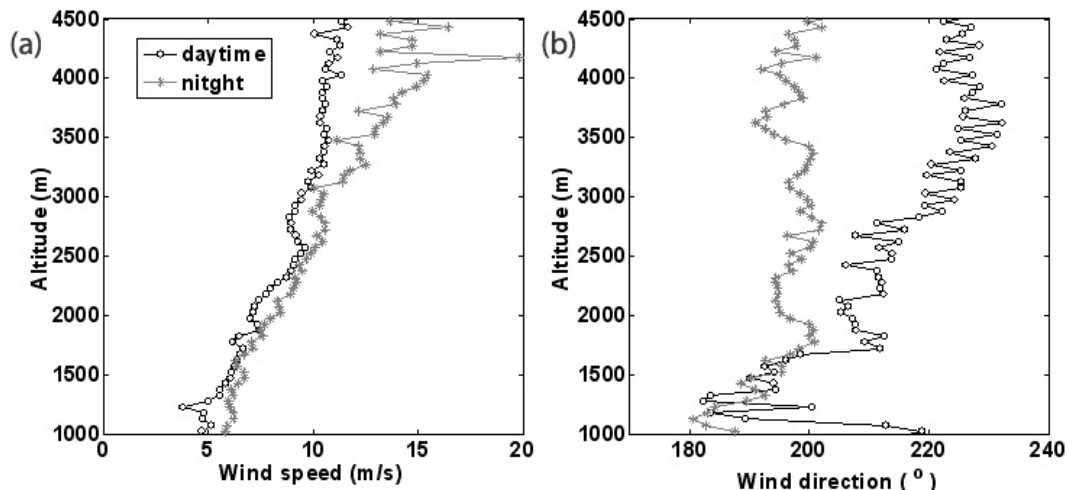


Fig. 12. Mean vertical profiles of **(a)** wind speed (m s^{-1}) and **(b)** wind direction ($^{\circ}$), obtained with radiosondes during BEARPEX 2009 campaign with heights from 1000 m to 4500 m. Gray stars denote the nighttime mean values (8 profiles launched between 10:00 ~ 17:00) and white circles represent mean daytime profiles (4 profiles launched for 00:00 ~ 03:00) during the BEARPEX campaign in 2009.

[Title Page](#)[Abstract](#)[Introduction](#)[Conclusions](#)[References](#)[Tables](#)[Figures](#)[◀](#)[▶](#)[◀](#)[▶](#)[Back](#)[Close](#)[Full Screen / Esc](#)[Printer-friendly Version](#)[Interactive Discussion](#)

**Estimating the
atmospheric
boundary layer
height over sloped**

W. Choi et al.

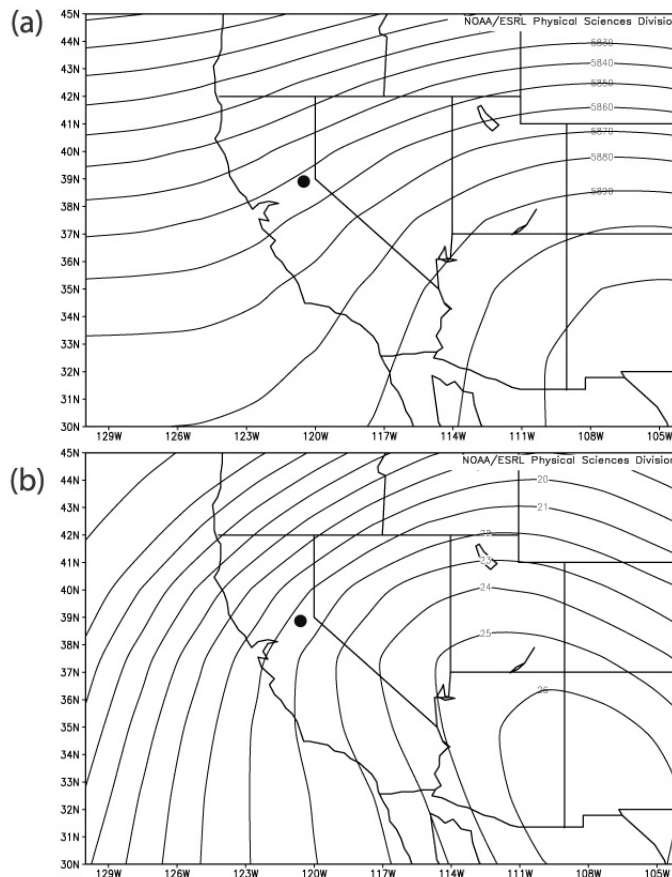


Fig. 13. Mean (a) geopotential height field at 500 mbar and (b) isotherms at 850 mbar during BEARPEX 2009 campaign (15 June ~ 30 July 2009). The x-axis is longitude (129° W ~ 105° W) and y-axis is latitude (30° N ~ 45° N). Black circle represents the location of Blodgett Forest. Data was obtained from the Earth System Research Laboratory of NOAA (NOAA, 2010).

[Title Page](#)[Abstract](#)[Introduction](#)[Conclusions](#)[References](#)[Tables](#)[Figures](#)[◀](#)[▶](#)[◀](#)[▶](#)[Back](#)[Close](#)[Full Screen / Esc](#)[Printer-friendly Version](#)[Interactive Discussion](#)